New Journal of Physics
The open access journal at the forefront of physics

Deutsche Physikalische Gesellschaft DPG IOP Institute of Physics

PAPER • OPEN ACCESS

An optomechanical heat engine with feedback-controlled in-loop light

IOP Publishing New J. Phys. 21 (2019) 093051 https://doi.org/10.1088/1367-2630/ab41e7

New Journal of Physics
The open access journal at the forefront of physics

Deutsche Physikalische Gesellschaft DPG
IOP Institute of Physics
Published in partnership with: Deutsche Physikalische Gesellschaft and the Institute of Physics

OPEN ACCESS

RECEIVED
1 May 2019

REVISED
22 August 2019

ACCEPTED FOR PUBLICATION
5 September 2019

PUBLISHED
24 September 2019

PAPER

An optomechanical heat engine with feedback-controlled in-loop light

Najmeh Etehadi Abari[1,2], **Giulia Vittoria De Angelis**[1], **Stefano Zippilli**[1] and **David Vitali**[1,3,4]

[1] School of Science and Technology, Physics Division, University of Camerino, I-62032, Camerino (MC), Italy
[2] Department of Physics, Faculty of Science, University of Isfahan, Hezar Jerib, 81746-73441, Isfahan, Iran
[3] INFN, Sezione di Perugia, I-06123, Perugia, Italy
[4] CNR-INO, Largo Enrico Fermi 6, I-50125, Firenze, Italy

E-mail: stefano.zippilli@unicam.it

Keywords: optomechanics, quantum heat engine, feedback

Abstract

The dissipative properties of an optical cavity can be effectively controlled by placing it in a feedback loop where the light at the cavity output is detected and the corresponding signal is used to modulate the amplitude of a laser field which drives the cavity itself. Here we show that this effect can be exploited to improve the performance of an optomechanical heat engine which makes use of polariton excitations as working fluid. In particular we demonstrate that, by employing a positive feedback close to the instability threshold, it is possible to operate this engine also under parameters regimes which are not usable without feedback, and which may significantly ease the practical implementation of this device.

1. Introduction

Heat engines convert thermal energy into work. A quantum heat engine uses a quantum system as working fluid. The practical realization of these devices is interesting as platforms for the experimental investigation of the thermodynamics of the quantum world and of non-equilibrium systems [1, 2].

Optomechanics [3] describes systems, which range from the nanoscale to macroscopic sizes, where the interaction between light and mechanical objects is exploited for enhanced metrology [4], and to explore the limits of quantum physics [5, 6]. Thermal machines based on optomechanical systems have been proposed and analysed in different configurations [7–15]. A specific example [7–9] makes use of hybridized polariton excitations as working fluid. This engine works in the strong optomechanical coupling regime where the normal modes of the system are superpositions of optical and mechanical excitations. This regime is in general not easily achievable and in some cases is inhibited by detrimental nonlinear processes, such as optical bistability or thermorefractive effects, which hamper the ability to carefully control the coupled dynamics of the systems. It has been shown [16] that feedback-controlled light [16–19] can be employed to significantly ease the onset of strong coupling in an optomechanical system. This suggests [20] that the feedback analysed in [19] can be used to enhance the efficiency of the quantum heat engine proposed in [7].

In this article we analyse the effect of feedback-controlled light on the performance of the polariton-based optomechanical heat engine discussed in [7–9]. We show that, with the aid of feedback, this engine can operate efficiently also when the system is not in the strong coupling regime and for parameters for which, in the absence of feedback, the engine is not functional.

The article is organized as follows. In section 2 we introduce the model of the optomechanical system driven by a feedback-controlled pump field. In section 3 we review the functioning of the quantum heat engine introduced in [7–9]. Then, in section 4 we discuss the effect of feedback on the performance of this device. In section 5 we present a variant of the engine which exploits the upper polariton mode as working fluid. Finally, section 6 is for the conclusions.

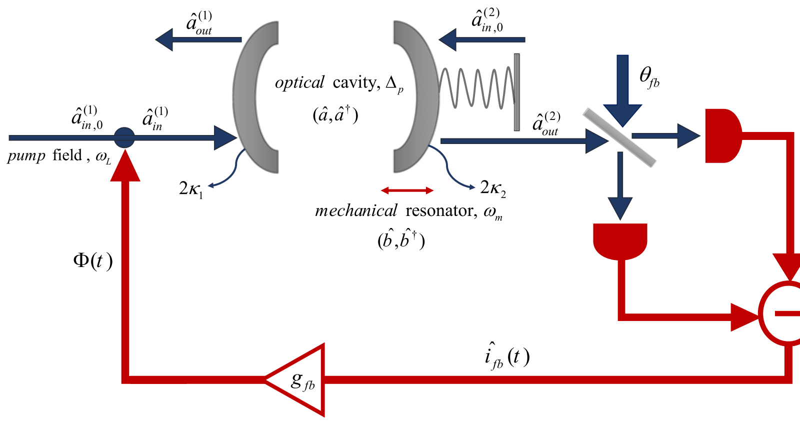

Figure 1. The feedback loop: a quadrature of the field, transmitted through a Fabry–Pérot cavity with a movable end mirror, is detected via homodyne detection at phase $\theta_{\rm fb}$, and the corresponding photocurrent is used to modulate the input field [19].

2. The model

In this work we consider an optomechanical device similar to the one discussed in [19], composed of an optical cavity with a moving end mirror placed within a feedback loop where the light transmitted through the cavity is detected and the corresponding signal is used to modulate the amplitude of the laser field which drives the system, see figure 1. In details, one resonant mode of the optical cavity at frequency ω_c and with decay rate κ_c, is coupled to a vibrational mode of the mirror, at frequency ω_m, which dissipates its energy at rate $\gamma \ll \omega_m$. The laser is at frequency ω_L and is detuned by $\Delta_p = \omega_L - \omega_c$ form the cavity resonance. We describe the system in terms of the standard linearized model for the fluctuations of the optical and mechanical variables about the corresponding average values [3] (this also implies that the cavity frequency includes the shift due to the optomechanical interaction). Specifically, assuming that the feedback does not affect the average laser intensity (this can be realized using a high-pass feedback response function which cuts the low-frequency components of the photocurrent [19]), the annihilation and creation operators for optical and mechanical excitations fulfil the quantum Langevin equations

$$\dot{\hat{a}} = -(\kappa_c - {\rm i}\Delta_p)\hat{a} - {\rm i}G(\hat{b} + \hat{b}^{\dagger}) + \sqrt{2\kappa_c}\,\hat{a}_{\rm in}, \tag{1}$$

$$\dot{\hat{b}} = -(\gamma + i\omega_m)\hat{b} - {\rm i}G(\hat{a} + \hat{a}^{\dagger}) + \sqrt{2\gamma}\,\hat{b}_{\rm in}, \tag{2}$$

where G is the linearized coupling strength, $\hat{b}_{\rm in}(t)$ is the noise operator for the mechanical resonator which describes thermal noise with $n_{\rm th}$ thermal excitations according to the correlation function $\langle \hat{b}_{\rm in}(t)\ \hat{b}^{\dagger}_{\rm in}(t')\rangle = (1 + n_{\rm th})\delta(t - t')$, $\hat{a}_{\rm in}(t)$ is the input noise operator for the cavity field which can be decomposed in terms of the noise operators $\hat{a}^{(1)}_{\rm in}(t)$ and $\hat{a}^{(2)}_{\rm in}(t)$ associated with the left and the right mirror respectively, as

$$\hat{a}_{\rm in}(t) = \frac{\sqrt{2\kappa_1}\ \hat{a}^{(1)}_{\rm in}(t) + \sqrt{2\kappa_2}\ \hat{a}^{(2)}_{\rm in}(t)}{\sqrt{2\kappa_c}}, \tag{3}$$

with κ_1 and κ_2 the corresponding decay rates, such that $\kappa_c = \kappa_1 + \kappa_2$. In turn, the noise operator $\hat{a}^{(1)}_{\rm in}(t)$ can be decomposed as the sum of the operator without feedback plus an additional term $\hat{\Phi}(t)$ due to the feedback $\hat{a}^{(1)}_{\rm in}(t) = \hat{a}^{(1)}_{\rm in,0}(t) + \hat{\Phi}(t)$. The input noise operators $\hat{a}^{(1)}_{\rm in,0}(t)$ and $\hat{a}^{(2)}_{\rm in}(t)$ describe vacuum fluctuations and are characterised by the correlation functions $\langle \hat{a}^{(1)}_{\rm in,0}(t)\ \hat{a}^{(1)\dagger}_{\rm in,0}(t')\rangle = \delta(t - t')$ and $\langle \hat{a}^{(2)}_{\rm in}(t)\ \hat{a}^{(2)\dagger}_{\rm in}(t')\rangle = \delta(t - t')$. The feedback term $\hat{\Phi}(t)$ depends on the feedback photocurrent [19]. In particular, if the feedback gain $\bar{g}_{\rm fb}$ is constant over a sufficiently large band of frequencies around the mechanical resonance, it can be approximated as $\hat{\Phi}(t) = \bar{g}_{\rm fb}\ \hat{i}_{\rm fb}(t - \tau_{\rm fb})$, such that it is proportional to the photocurrent $\hat{i}_{\rm fb}(t)$ at an earlier time determined by the feedback delay time $\tau_{\rm fb}$ [19, 20], so that

$$\hat{a}^{(1)}_{\rm in}(t) = \hat{a}^{(1)}_{\rm in,0}(t) + \bar{g}_{\rm fb}\ \hat{i}_{\rm fb}(t - \tau_{\rm fb}). \tag{4}$$

The photocurrent resulting from the homodyne detection of the field at the output of the second mirror is expressed as [19]

$$\hat{i}_{\rm fb}(t) = \sqrt{\eta_{\rm d}}\ \hat{X}^{(\theta_{\rm fb})}_{\rm out,fb}(t) + \sqrt{1 - \eta_{\rm d}}\ \hat{X}_{\nu}(t), \tag{5}$$

where $\theta_{\rm fb}$ is the phase of the local oscillator, η_d is the detection efficiency, $\hat{X}_\nu(t)$ is an operator representing additional noise due to the inefficient detection, which satisfies the relation $\langle \hat{X}_\nu(t)\hat{X}_\nu(t')\rangle = \delta(t-t')$, and $\hat{X}^{(\theta_{\rm fb})}_{\rm out,fb}(t) = {\rm e}^{-{\rm i}\theta_{\rm fb}}\,\hat{a}^{(2)}_{\rm out}(t) + {\rm e}^{{\rm i}\theta_{\rm fb}}\,\hat{a}^{(2)\dagger}_{\rm out}(t)$ is the detected field quadrature at phase $\theta_{\rm fb}$, with corresponding annihilation operator determined by the standard input–output relation [21]

$$\hat{a}^{(2)}_{\rm out}(t) = \sqrt{2\kappa_2}\;\hat{a}(t) - \hat{a}^{(2)}_{\rm in}(t). \tag{6}$$

According to equations (4) and (5) this operator is calculated at the delayed time $\hat{a}^{(2)}_{\rm out}(t-\tau_{\rm fb})$ and, in the regime of large detuning with respect to the optomechanical coupling constant and cavity decay rate, i.e. $|\Delta_p| \gg G,\ \kappa_c$, it is convenient to rewrite it as a product of two terms (a slowly varying one and fast oscillating one) as $\hat{a}_{\rm out}(t-\tau_{\rm fb}) = \hat{\tilde{a}}_{\rm out}(t-\tau_{\rm fb})\,{\rm e}^{-{\rm i}\Delta_p(t-\tau_{\rm fb})}$. Whenever the delay time is much shorter than both the characteristic time of the interaction $1/G$ and the decay time of the cavity $1/2\kappa_c$, i.e. $\tau_{\rm fb} < 1/G,\ 1/2\kappa_c$, we can ignore the delay time dependence of the slow part $\hat{\tilde{a}}_{\rm out}(t-\tau_{\rm fb})$ and then rewrite the output operator as

$$\hat{a}_{\rm out}(t-\tau_{\rm fb}) \simeq \hat{\tilde{a}}_{\rm out}(t)\;{\rm e}^{-{\rm i}\Delta_p t}\;{\rm e}^{{\rm i}\Delta_p\tau_{\rm fb}} = \hat{a}_{\rm out}(t)\;{\rm e}^{{\rm i}\Delta_p\tau_{\rm fb}}. \tag{7}$$

In this situation the delay-time dependence of the photocurrent in equation (4) can be approximated as a phase factor such that

$$\hat{\rm i}_{\rm fb}(t-\tau_{\rm fb}) = \sqrt{\eta_d}\;({\rm e}^{-{\rm i}\phi}\;\hat{a}^{(2)}_{\rm out}(t) + {\rm e}^{{\rm i}\phi}\;\hat{a}^{(2)\dagger}_{\rm out}(t)) + \sqrt{1-\eta_d}\;\hat{X}_\nu(t), \tag{8}$$

where we have introduced the global phase $\phi \equiv \theta_{\rm fb} - \Delta_p\tau_{\rm fb}$.

By using equations (6), (4)and (8) and assuming $\phi = 0$ (this can be achieved by properly adjusting the value of $\theta_{\rm fb}$ depending on the value of detuning), we can rewrite the equation for the cavity operator (1) as

$$\dot{\hat{a}}(t) = -(\kappa_{\rm fb} - {\rm i}\Delta_p)\;\hat{a}(t) + (\kappa_c - \kappa_{\rm fb})\;\hat{a}^\dagger(t) - {\rm i}G\;[\hat{b}(t) + \hat{b}^\dagger(t)] + \sqrt{2\kappa_{\rm fb}}\;\hat{a}_{\rm in,fb}(t), \tag{9}$$

where we have introduced the feedback-modified cavity decay rate

$$\kappa_{\rm fb} = \kappa_c - 2\bar{g}_{\rm fb}\sqrt{\eta_d\kappa_1\kappa_2} \tag{10}$$

and the corresponding noise operator

$$\hat{a}_{\rm in,fb}(t) = \frac{1}{\sqrt{2\kappa_{\rm fb}}}\{\sqrt{2\kappa_1}\;\hat{a}^{(1)}_{\rm in,0}(t) + \sqrt{2\kappa_2}\;\hat{a}^{(2)}_{\rm in}(t) - \bar{g}_{\rm fb}\sqrt{2\eta_d\kappa_1}\;[{\rm e}^{-{\rm i}\phi}\hat{a}^{(2)}_{\rm in}(t) + {\rm e}^{{\rm i}\phi}\hat{a}^{(2)\dagger}_{\rm in}(t)]$$
$$+\;\bar{g}_{\rm fb}\sqrt{2(1-\eta_d)\kappa_1}\;\hat{X}_\nu(t),\}, \tag{11}$$

which describes additional effective thermal noise characterised by the correlation relations

$$\langle \hat{a}^\dagger_{\rm in,fb}(t)\;\hat{a}_{\rm in,fb}(t')\rangle = n_{\rm opt,fb}\;\delta(t-t'), \tag{12}$$

$$\langle \hat{a}_{\rm in,fb}(t)\;\hat{a}_{\rm in,fb}(t')\rangle = 0, \tag{13}$$

with the feedback-mediated number of thermal excitations defined as

$$n_{\rm opt,fb} = \frac{(\kappa_c - \kappa_{\rm fb})^2}{\eta_d\kappa_c\kappa_{\rm fb}}. \tag{14}$$

This shows that, the feedback-controlled system behaves as an effective optomechanical system with modified cavity decay rate $\kappa_{\rm fb}$, under the effect of additional noise with a finite number of thermal excitations $n_{\rm opt,fb}$ and of an additional parametric driving term with strength $\kappa_c - \kappa_{\rm fb}$ (see equation (9)). The values of both $\kappa_{\rm fb}$ and $n_{\rm opt,fb}$ are controllable via the feedback gain $\bar{g}_{\rm fb}$ according to the relations (10) and (14). This allows one to operate the same system under different parameter regimes [16–19]. In particular when the feedback is operated close to its instability threshold, namely when the effective cavity decay rate becomes very small ($\kappa_{\rm fb} \to 0$), also a weakly coupled system may exhibits the typical features of strongly coupled systems such as normal mode splitting [16].

3. The polariton-based optomechanical heat engine

References [7–9] describe a quantum heat engine which makes use of polariton excitations in an optomechanical system (without feedback) as working fluid. This device requires strong optomechanical coupling and resolved sideband regime $\omega_m,\ G \gg \kappa_c$ for its functioning. And works at red detuning, where the laser frequency is lower than the cavity frequency so that the optical and mechanical mode can exchange coherently their excitations. Only in this regime the hybridised polariton excitations (the excitations of the normal modes of the system) become relevant. The engine focuses on the lower polariton mode and realises an Otto cycle formed by two adiabatic and two isochoric processes. Specifically it works as follows (see figure 2). The lower polariton frequency plays the role of the volume of the working fluid (similar to other single oscillator engines [1, 2]) and it can be controlled via the laser detuning. This is the central tool used to operate the engine through the four strokes of the cycle. At large detuning the lower polariton is phonon-like and it is in thermal contact with the hot

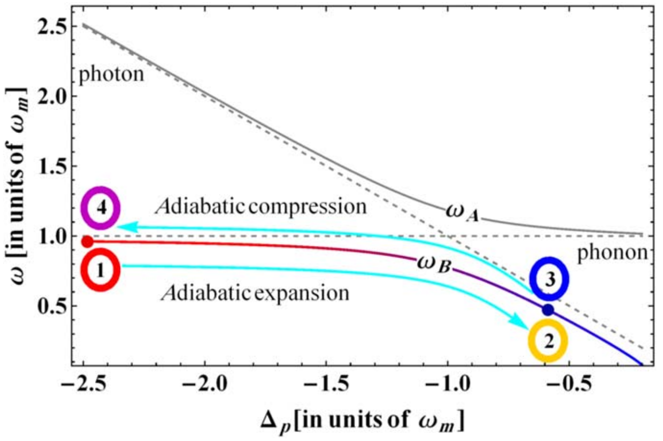

Figure 2. Frequency of the two polaritons (upper ω_A and lower ω_B) of the optomechanical system as a function of the cavity detuning Δ_p in the red-detuned case $\Delta_p < 0$ (the optomechanical coupling strength is $G = 0.05\ \omega_m$). The dashed curves correspond to the frequencies of the non-interacting modes. In the plot we have indicated the position of the four nodes of the Otto cycle operated on the lower polariton. The strokes from node 1 to 2 and from 3 to 4 correspond to the adiabatic processes. The strokes from node 2 to 3 and from 4 to 1 take place at constant detuning and correspond to the isochoric processes.

mechanical thermal bath (see figure 2). A fast change of the detuning brings the laser closer to the cavity resonance, passing through the red mechanical sideband, until the polariton becomes photon-like and comes into contact with the cold (zero temperature) optical bath. This variation of the detuning realizes the first adiabatic process from 1 to 2 (see figure 2). Hence it has to be sufficiently fast in order to avoid dissipation. However, at the same time, it has to be sufficiently slow in order to avoid non-adiabatic transitions to the upper polariton mode. This means that the duration τ_1 of this process must fulfil the conditions $1/G \ll \tau_1 \ll 1/\kappa_c$ (note that the linearized optomechanical coupling is assumed constant during the cycle; this can be achieved by properly controlling the pump intensity during the adiabatic processes [7–9]). After the adiabatic process, the detuning is kept fixed at the value closest to the cavity resonance for a time $\tau_2 \gg 1/\kappa_c$ until the lower (photon-like) polariton thermalizes with the optical reservoir realising the first isochoric process. This process has to be sufficiently short ($\tau_2 \ll 1/\gamma$) in order to avoid mechanical dissipation of the upper(phonon-like) polariton which should not contribute to the variation of the system energy during the cycle. The second adiabatic process is realized by sweeping back the detuning to the initial value over a time $\tau_3 = \tau_1$ so to guarantee the adiabaticity of the process. Now, the lower polariton is again phonon-like and in the second isochoric process it thermalizes with the thermal mechanical bath, over a time $\tau_4 \gg 1/\gamma$. The upper polariton, instead, does not change significantly its number of excitations during the full cycle.

4. The feedback-enabled heat engine

A critical requirement in this device is the ability to realise the adiabatic processes which needs a sufficiently large difference between G and κ_c. This is the regime of strong coupling that, although reached in a few systems [22, 23], is not straightforward to achieve, and in certain cases it is inhibited by the onset of detrimental nonlinear effects [16]. As discussed in [16], the feedback that we have described above seems particularly fit for this purpose, and can be exploited to ease the realisation of this engine. In particular, on the one hand the feedback loop enables one to reduce the cavity bandwidth and to bring a system into the strong coupling regime even if naturally it is weakly coupled; on the other hand it adds extra noise to the cavity, corresponding to a finite number of thermal photonic excitations $n_{\mathrm{opt,fb}}$. In order to realize the heat engine that works on the lower polariton, the cycle should work between a cold photonic reservoir and a hot phononic reservior. This means that the Otto cycle that we have discussed can be effective as long as $n_{\mathrm{opt,fb}} < n_{\mathrm{th}}$, which implies (see equation (14)) that κ_{fb} cannot be too small. Furthermore, a difference between the model of [7, 8] and the feedback-controlled system introduced in section 2 is the additional parametric driving in the latter (see equation (9)). However when the system is in the resolved sideband regime its effect is very small. Hence, neglecting the parametric term we can perform an analysis similar to the one discussed above also in the case of feedback. And we can state that, when one utilises feedback, the engine can work efficiently when the duration of the four strokes fulfil the following set of relations

$$\frac{1}{G} \ll \tau_1, \tau_3 \ll \frac{1}{\kappa_{fb}} \ll \tau_2 \ll \frac{1}{\gamma} \ll \tau_4, \tag{15}$$

and

$$n_{\text{opt,fb}} < n_{\text{th}}. \tag{16}$$

If the cycle operates optimally with ideal adiabatic passages, then it realises a perfect Otto cycle where, in the adiabatic processes, the system exchanges energy with the environment in terms of work without transferring heat, instead, in the isochoric processes the system exchanges only heat and thermalizes with the environment (see appendix C for a definition of heat and work that applies to this system). In this case the heat and the work in each stroke is given by the difference between the system's energy at the beginning and at the end of each stroke $\Delta E_{i\to j} = E_j - E_i$ (for $i, j = 1, 2, 3, 4$), where, denoting with the label A the upper polariton and with B the lower one, the system energy is given by $E = \hbar\,(\omega_A N_A + \omega_B N_B)$, with ω_x and N_x (for $x \in \{A,\ B\}$) the frequency and the number of polariton excitations respectively. The polariton A is initially photon-like and its frequency is given by the initial cavity detuning $\omega_A \sim |\Delta_i|$, with corresponding number of excitations $N_A \sim n_{\text{opt,fb}}$. The polariton B, instead, is initially phonon like with frequency $\omega_B \sim \omega_m$ and $N_B \sim n_{\text{th}}$ excitations. At the end of the first adiabatic process A becomes phonon-like, at frequency $\omega_A \sim \omega_m$, and B photon-like with a frequency close to the corresponding cavity detuning $\omega_B \sim |\Delta_f|$. Then, in the isochoric process the polariton B thermalizes with the feedback-mediated optical bath, while A should remain with its initial number of excitations. Then, in the second adiabatic process the polariton frequencies return to their initial values, and finally in the second isochoric process, polariton B returns to its initial value of excitations (note that during an ideal cycle the number of excitations of the polariton A should remain constant). Hence ideally the changes of energy (and the corresponding heat Q and work W) in the four strokes, are

$$\begin{aligned}
W_{1\to 2} &= \Delta E_{1\to 2} \sim \hbar\,(|\Delta_f|\ n_{\text{th}} + \omega_m\ n_{\text{opt,fb}}) - \hbar\,(\omega_m\ n_{\text{th}} + |\Delta_i|\ n_{\text{opt,fb}}) < 0,\\
Q_{2\to 3} &= \Delta E_{2\to 3} \sim \hbar|\Delta_f|\ n_{\text{opt,fb}} - \hbar|\Delta_f|\ n_{\text{th}} < 0,\\
W_{3\to 4} &= \Delta E_{3\to 4} \sim \hbar\,(\omega_m\ n_{\text{opt,fb}} + |\Delta_i|\ n_{\text{opt,fb}}) - \hbar\,(|\Delta_f|\ n_{\text{opt,fb}} + \omega_m\ n_{\text{opt,fb}}) > 0,\\
Q_{4\to 1} &= \Delta E_{4\to 1} \sim \hbar\omega_m\ n_{\text{th}} - \hbar\omega_m\ n_{\text{opt,fb}} > 0.
\end{aligned} \tag{17}$$

The negative work in the first stroke indicates that the work is performed by the system, while the positive heat in the fourth stroke indicates that the heat is absorbed by the system. The efficiency of the cycle is given by the ratio $\eta = -\mathrm{W}_{\text{tot}}/Q_{\text{abs}}$ between the total work $W_{\text{tot}} = W_{1\to 2} + W_{3\to 4}$ and the absorbed heat $Q_{\text{abs}} = Q_{4\to 1}$, that is,

$$\eta = \frac{-(W_{1\to 2} + W_{3\to 4})}{Q_{4\to 1}} \sim 1 - \frac{|\Delta_f|}{\omega_m}. \tag{18}$$

Note that during the adiabatic processes part of the work is also done by and on the polariton A (respectively in the first and second adiabatic process). However, since the number of excitations does not change the net contribution to the total work due to polariton A is zero.

4.1. Results

A more accurate estimate of the efficiency and of the work performed by this engine can be computed by focusing on the steady state properties of the lower polariton B alone at the end of each stroke, but still assuming perfect adiabatic processes and constant population of the upper polariton throughout the whole cycle. This allows to better estimate the expected performance of the engine by taking into account also the effects of the optomechanical interaction at large and small detuning. Specifically, equations (2) and (9) can be used to evaluate the steady state correlation matrix $\mathcal{C}_{ss}$ of the system (see appendix A for details); moreover, the populations and the frequencies of the polariton mode B can be estimated by transforming the correlation matrix to the polariton bases, which determines the normal modes of the system Hamiltonian as discussed in appendix B. This allows to estimate the energy associated to the polariton B at the beginning and end of each stroke ($E_{B,j} = \hbar\omega_{B,j}\ N_{B,j}$ for $j = 1, 2, 3, 4$) and to estimate the corresponding work and heat (such as $W_{\text{tot}} \sim -(E_{B,2} - E_{B,1} + E_{B,4} - E_{B,3})$ and $Q_{\text{abs}} \sim E_{B,1} - E_{B,4}$). The corresponding results are reported in figure 3. They show that the optimal performance of the engine are achieved at small Δ_p and G [7, 8]. In this regime however our estimate are likely to be inaccurate. In fact, on the one hand, at vanishing G the time for the adiabatic passage needs to be extremely long (longer then the dissipation time), and on the other hand at small Δ_p the effect of the parametric term can become important (in fact at very small Δ_f the system is unstable (see appendix C) as indicated by the white areas in figure 3). In order to address this issue more rigorously we have analysed the full dynamics of the system.

An in-depth study of the efficiency of the engine is achieved by solving the quantum Langevin equations (2) and (9), and computing the time evolution of the energy exchanged between the system and the environment in terms of heat and work as discussed in appendix C. Specifically, these quantities can be expressed in terms of the correlation functions of the system operators, the dynamics of which can be computed by standard techniques

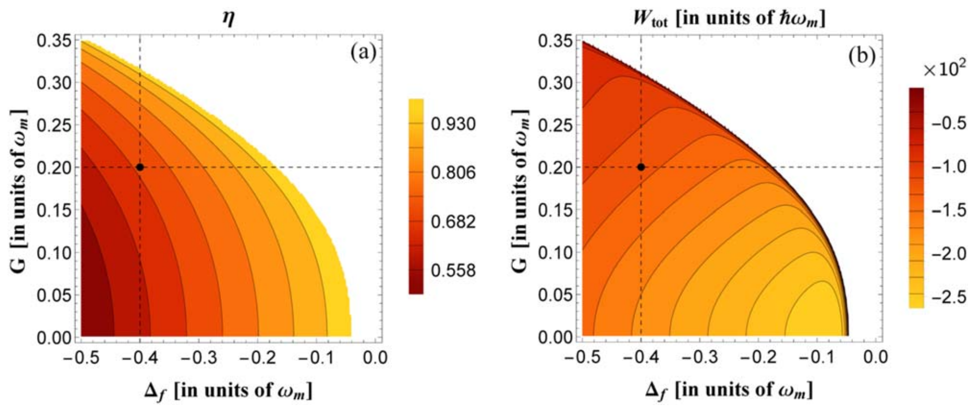

Figure 3. (a) Thermal efficiency η and (b) total work W_{tot} done by the engine (operated on the lower polariton) as a function of the smallest detuning Δ_f and the optomechanical coupling strength G, evaluated in terms of the steady-state energy corresponding to the lower polariton mode at each node of cycle, assuming perfect adiabatic processes and constant excitations of the upper polariton mode. The white areas indicate the parameter regime at which the system is unstable (see appendix C). The dots indicate the parameters used for the results in figures 5 and 6. The other parameters are $\Delta_i = -3\omega_m$, $2\kappa_c = 0.1\omega_m$, $2\gamma = 10^{-4}\omega_m$, and $n_{\text{th}} = 300$. The feedback is set in order to achieve the effective cavity decay rate $2\kappa_{\text{fb}} = 0.015\omega_m$, corresponding to an effective number of thermal photons $n_{\text{opt,fb}} \approx 8$ (see equation (14)).

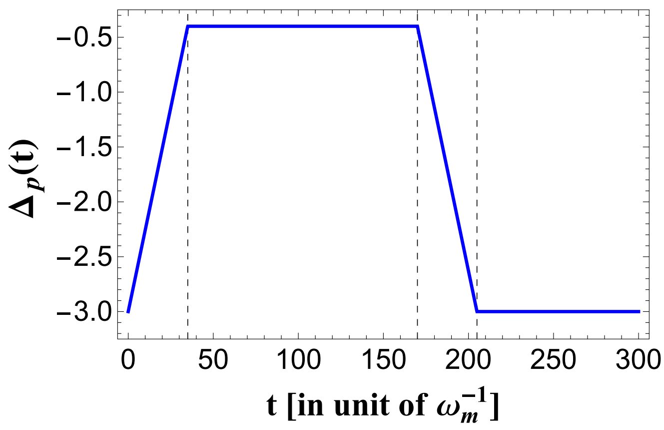

Figure 4. Time evolution of the detuning Δ_p. The vertical dashed lines indicate the end and the beginning of each stroke. The last stroke is not shown completely because it is very slow due to the small mechanical damping rate γ. During the last stroke the Δ_p remains constant.

(see appendix A). Hereafter we report and discuss the result of this numerical analysis when the cavity detuning Δ_p is changed in time, in order to realise the Otto cycle, according to the relation

$$\Delta_p(t) = \begin{cases} \frac{\Delta_f - \Delta_i}{t_1 - t_0}(t - t_0) + \Delta_i, & t_0 \leqslant t < t_1 \\ \Delta_f, & t_1 \leqslant t < t_2 \\ \frac{\Delta_i - \Delta_f}{t_3 - t_2}(t - t_2) + \Delta_f, & t_2 \leqslant t < t_2 \\ \Delta_i, & t_3 \leqslant t \leqslant t_4. \end{cases} \tag{19}$$

In details (see figure 4), in the first stroke the detuning is changed linearly from the initial value Δ_i to Δ_f. Then it is kept constant at the value Δ_f. In the third stroke it changes linearly back to the initial value. And finally, in the last stroke, it remains constant at the value Δ_i. The duration of each stroke is $\tau_j = t_1 - t_{j-1}$, for $j = 1, 2, 3, 4$.

In figure 5 we report the results evaluated for an optomechanical coupling G of the same order of the cavity decay rate κ_c. In this case the engine described in [7, 8] has low efficiency. Here we utilize feedback to effectively reduce the cavity linewidth and reach the regime of strong coupling [16] and significantly enhance the performance of the engine. Figure 5(a) shows that the lowest polariton B plays the main role in the dynamics of the system, and we can ignore the dynamics of the polariton A as the variation of its excitations is relatively small during each stroke of the Otto cycle. At the beginning of the process, the number of excitations of the upper and lower polariton modes, N_A and N_B, are almost equal to the number of photons N_a and phonon N_b respectively.

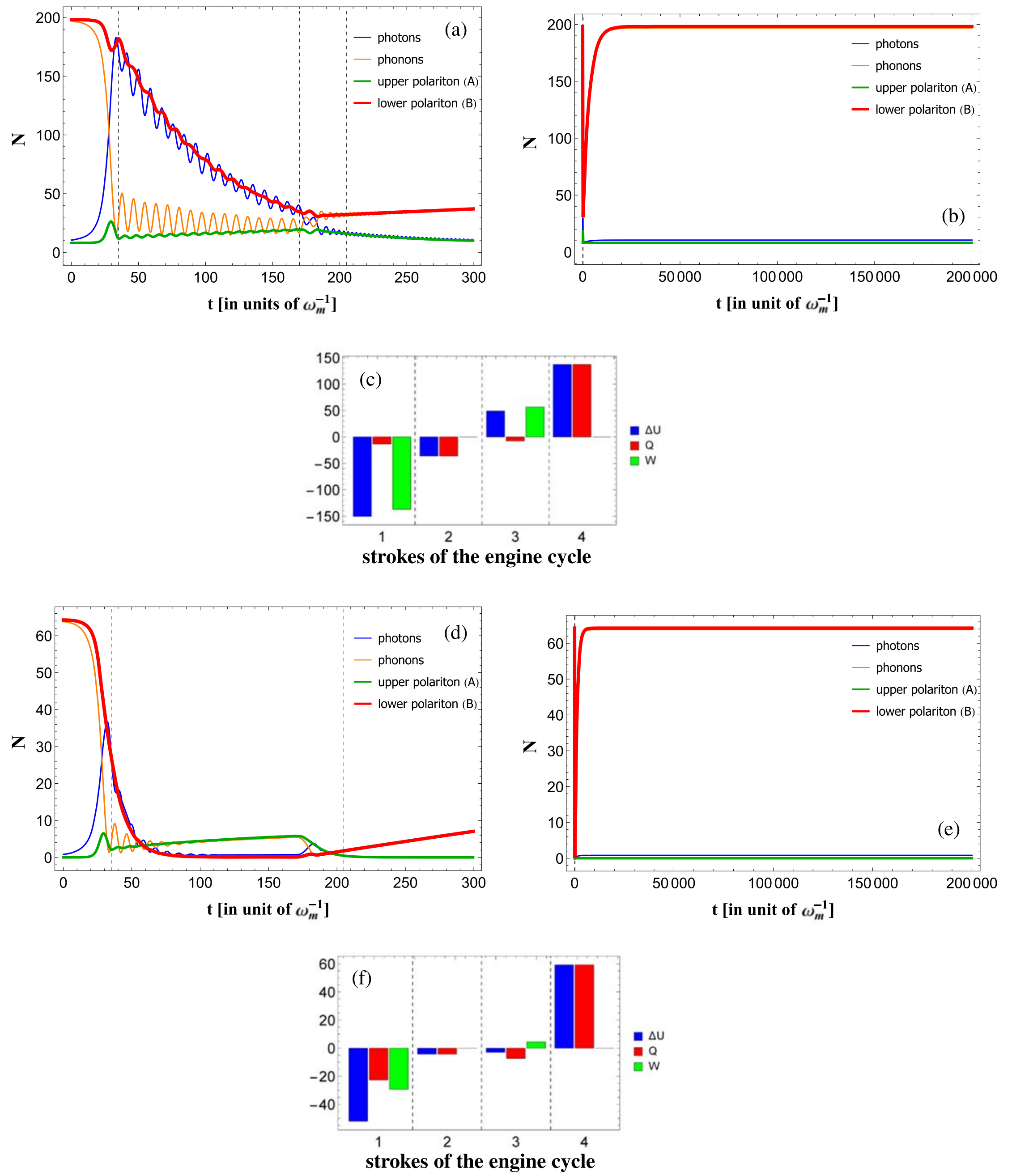

Figure 5. (a), (b), (d), (f) Time evolution of the populations of the polariton modes, N_B (red line) and N_A (green line), and of the photonic (N_a, blue line) and phononic modes (N_b, orange line) during a loop of the engine cycle (with initial state given by the system steady state at the initial detuning) with (a), (b) and without (d), (e) feedback. (a) and (d) show the dynamics in the first three strokes. (b) and (d) show a longer time scale that highlight the slow thermalization in the fourth stroke. Corresponding energy change (blue), heat exchanged (red) and work performed (green) during each stroke of the cycle. The duration of each stroke is $\tau_1 = \tau_3 = 35\omega_m^{-1}$, $\tau_2 = 135\omega_m^{-1}$ and $\tau_4 = 20/\gamma$. The other parameters are as in figure 3.

The numbers of polaritons N_A and N_B remain almost constant during the first adiabatic passage (while at the same time the phonon and photon numbers exchange their values). In the second stroke the photon-like B-polaritons decay due to cavity dissipation (the oscillations of the photon and phonon populations are due to the optomechanical coupling). In the third stroke the polariton mode B comes back to its phonon-like character, and then it slowly thermalizes to its initial population. The final thermalization is shown in plots (b) and (e) because it is very slow due to the small mechanical damping rate γ. This behaviour is consistent with that of an Otto cycle as discussed in section 4 [7, 8]. It is also worth to notice that the population of polariton A remains small throughout the whole cycle, indicating that it plays a minor role in the energy exchanges and hence in the functioning of the engine. Figure 5(c) shows the changes in energy, work and heat in each stroke. As expected for an Otto cycle, the first and third strokes (the adiabatic passages) are mainly associated with work production, while heat is exchanged mainly in the isochoric processes (second and fourth strokes). In particular, the system

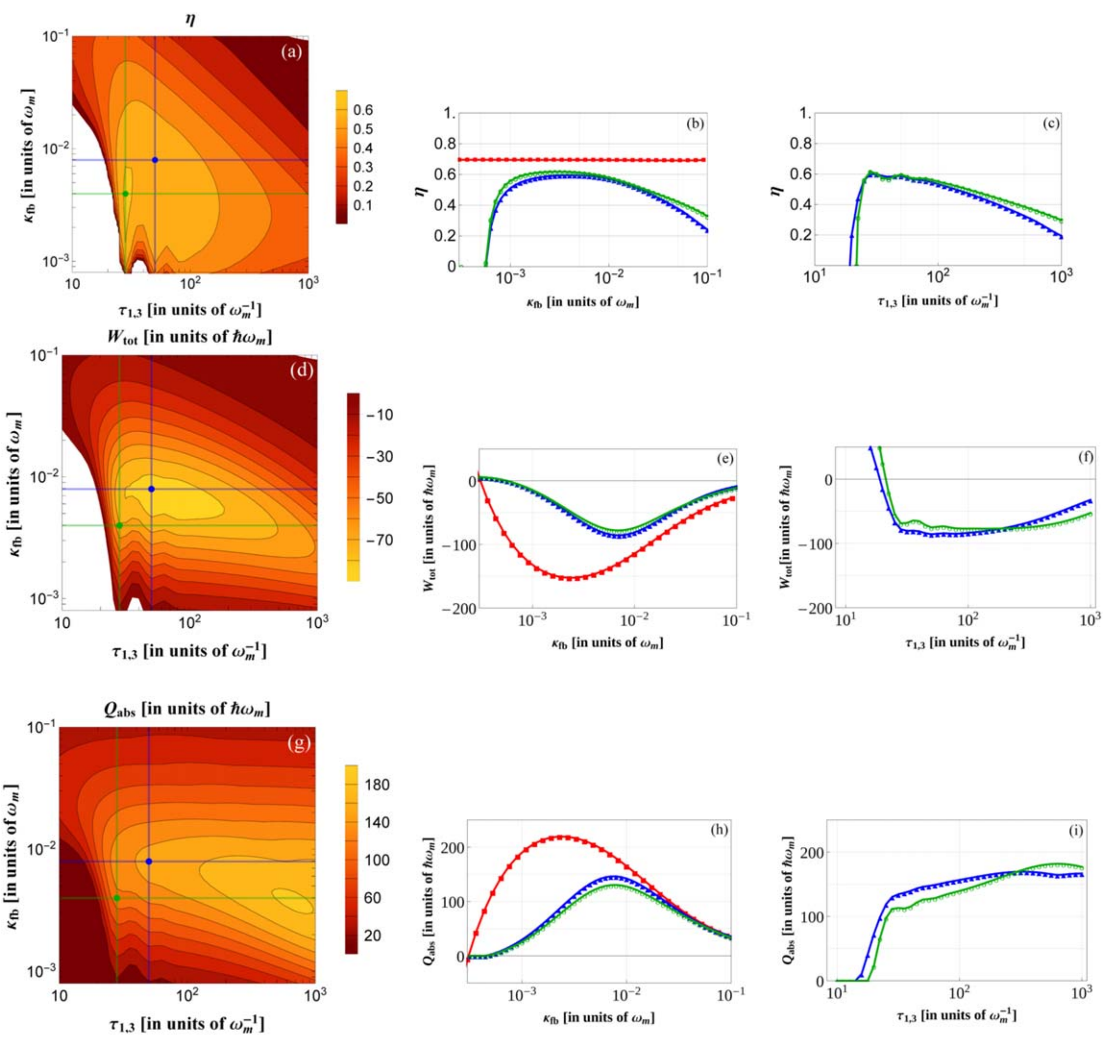

Figure 6. (a)–(c): Efficiency of the quantum engine; (d)–(f): total work; (g)–(i): absorbed heat during the cycle, versus κ_{fb} and τ_1 $(= \tau_3)$, evaluated by computing the system time evolution as discussed in appendix C. The plots in the second column report the values of efficiency (b), work (e) and heat (h) as a function of κ_{fb}, for the value of τ_1 $(= \tau_3)$ indicated by the vertical lines in the corresponding contour plots. The green and blue lines correspond to the values that maximize efficiency and work respectively. The red lines correspond to the quantities calculated considering stationary states as in figure 3. The plot in the third column report the values of efficiency (c), work (f) and heat (i) as a function of τ_1 $(= \tau_3)$, for the value of κ_{fb} indicated by the horizontal lines in the corresponding contour plots. The other parameters are the same as those used in figure 5.

produces work in the first stroke, while it absorbs heat in the fourth stroke. The marginal imperfections of figure 5(c) (finite heat exchanges in the first and third stroke) are due to non-ideal adiabatic processes [20]. As a comparison we plot in figures 5(d)–(f) the corresponding results achievable with the same system when the feedback is off. In this case the cavity dissipation is too large and the population of the polariton mode B decreases significantly in the first stroke, the work performed is strongly reduced and the corresponding thermal efficiency is much lower.

It is instructive to analyse the performance of the engine in terms of its efficiency, performed work and absorbed heat as a function of the two most critical time scales of the engine dynamics, namely the effective decay rate κ_{fb} and the duration of the adiabatic processes τ_1 $(=\tau_3)$. These results are shown in figure 6. The contour plots highlight that although maximum efficiency and maximum work are not achieved for the same parameters (see the dots in the contour plots), the corresponding values are relatively stable and the results achieved when η is maximum are very close to those corresponding to maximum $-W_{\text{tot}}$. The work is maximized at intermediate values of both κ_{fb} and τ_1, as a compromise between the opposite requirements described by the hierarchy relations (15). The white areas in the contour plots indicate the parameters in which the engine is not functional. Namely for these parameters the total work become positive (indicating that the work is done on the system and not by the system). Plots (b), (c), (e), (f), (h) and (i) represent the values of η, W_{tot} and Q_{abs}, along the vertical and horizontal lines depicted in the contour plots. The red lines in the plots (b), (e) and (h) correspond to the approximate results evaluated following the procedure used also for the results reported in figure 3. We observe that the exact result approaches the estimates close to the optimal values.

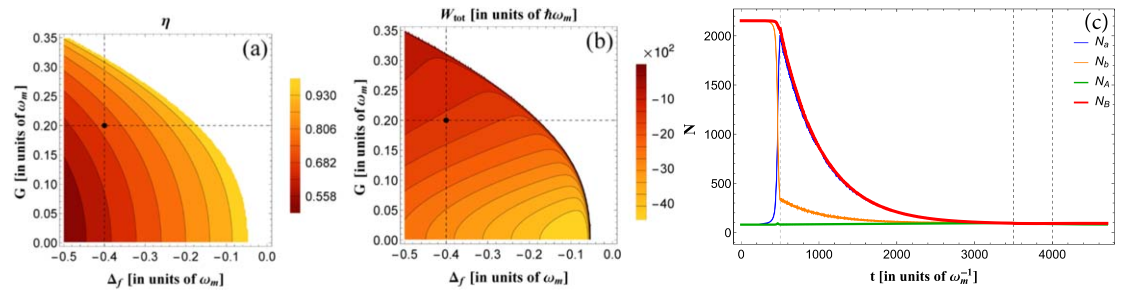

Figure 7. (a) Thermal efficiency η and (b) total work W_{tot} done by the engine as in figure 3 but with $2\gamma = 10^{-7}\,\omega_m$, and $n_{th} = 5000$, $\Delta_i = -10\omega_m$, $2\kappa_{fb} = 2 \times 10^{-3}\,\omega_m$ ($n_{opt,fb} \approx 80$). (c) the time evolution of the population of the polariton and bare modes for the parameters corresponding to the dot in plot (a) and (b) and with $\tau_1 = \tau_3 = 500\,\omega_m^{-1}$, $\tau_2 = 3/\kappa_{fb}$ and $\tau_4 = 20/\gamma$.

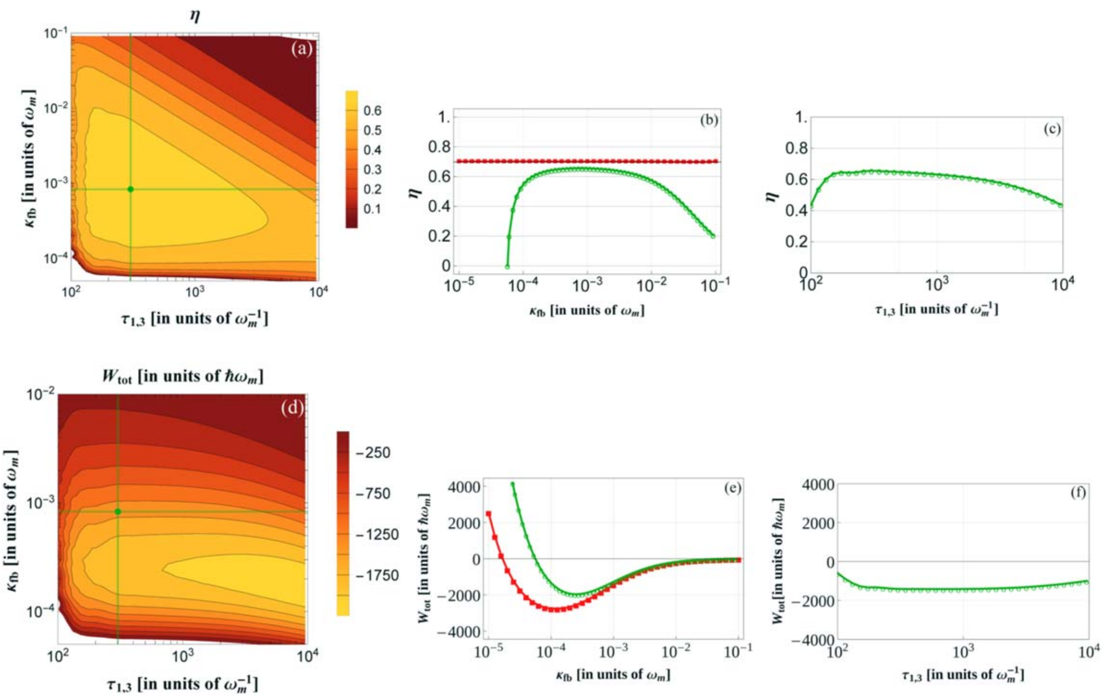

Figure 8. (a)–(c): Efficiency of the quantum engine; (d)–(f): total work versus κ_{fb} and $\tau_1\,(=\tau_3)$, evaluated by computing the system time evolution as discussed in appendix C. The plot in the second column report the values of efficiency (b) and work (e) as functions of κ_{fb}, for the value of $\tau_1\,(=\tau_3)$ indicated by the vertical lines in the contour plots. The red lines correspond to the quantities calculated considering stationary states as in figure 7. The plot in the third column report the values of efficiency (c) and work (f) as a function of $\tau_1\,(=\tau_3)$, for the value of κ_{fb} indicated by the horizontal lines in the contour plots. The other parameters are the same as those corresponding to figure 7(c).

The work done by this engine can be easily increased by using an higher temperature phonon reservoir. This is shown in figure 7, where the number of thermal excitations is increased with respect to the situation of figure 3. In these results we have also considered a larger value of the initial detuning, which implies a longer time of the adiabatic processes, and in turn requires a smaller value of the cavity decay rate. The corresponding time evolution of the populations of the system modes is shown in figure 7(c) and describes the expected behaviour discussed in section 3. Figure 8 instead displays the corresponding results as a function of the effective cavity decay rate κ_{fb} and of the duration of the adiabatic processes and $\tau_1\;(=\tau_3)$ evaluated by solving the dynamics of the full model. We observe that while the efficiency of the engine is only slightly larger than the one achieved with the parameters of figure 5, the work done by the system is significantly larger, and it achieves its optimal value when both κ_{fb} and τ_1 fulfil the relations (15).

Figure 3 and 7 show that the optimal performance of the engine is expected for small optomechanical coupling G and small final detuning Δ_f, and this is confirmed by the results reported in figures 9 and 10. For the parameters used in figure 9 the system follows more closely the ideal transformations described in section 3. Specifically figure 9(c) shows the time evolution of the populations of the system modes, with an almost perfect exchange of excitations between cavity and mechanical resonator in the first stroke and with N_A which remains

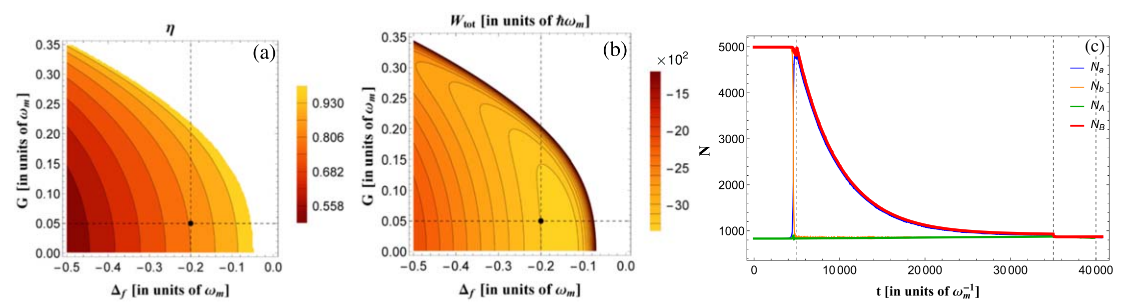

Figure 9. The same as in figure 7 with $2\kappa_{\mathrm{fb}} = 2 \times 10^{-4}\,\omega_m$ ($n_{\mathrm{opt,fb}} \approx 830$) and $\tau_1 = \tau_3 = 5000\,\omega_m^{-1}$.

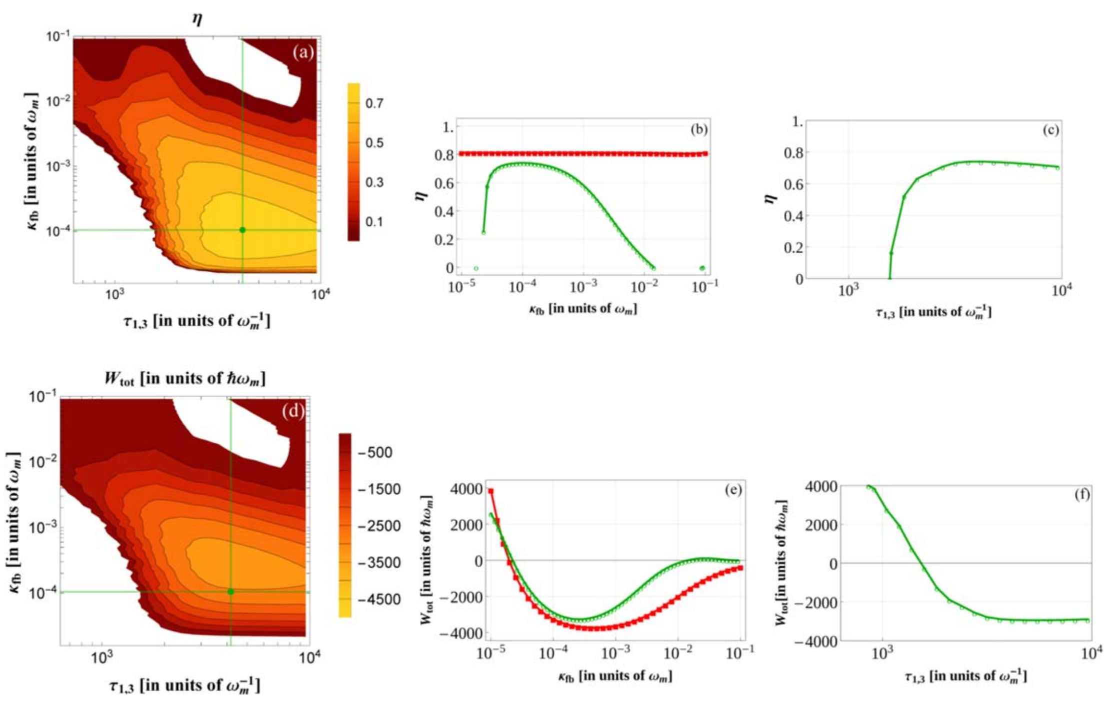

Figure 10. The same as in figure 8 but for the parameters corresponding to figure 9(c).

essentially constant. Figure 10 shows that both the efficiency and the work done by the engine are significantly enhanced even if the system (without feedback) is not strongly coupled.

5. The Otto cycle on the upper polariton

In the previous section we have studied the thermodynamical properties of an Otto cycle operated on the lower polariton B. A similar device can be implemented also using the upper polariton A if the following conditions are fulfilled

$$\frac{1}{G} \ll \tau_1, \tau_3 \ll \frac{1}{\gamma} \ll \tau_2 \ll \frac{1}{\kappa_{fb}} \ll \tau_4, \tag{20}$$

$$n_{\mathrm{opt,fb}} > n_{\mathrm{th}}, \tag{21}$$

such that the cavity effectively decay over the longest time scale and is coupled to the hot bath, meaning that the roles of the hot and cold bath are now exchanged. These conditions can be, in principle, realized with the help of feedback in a system with not to small mechanical dissipation rate γ and low thermal fluctuations. The four strokes of the cycle are then similar to what we have discussed above, and can be realized with a similar variation of the detuning (19), but with the roles of photonic and phononic excitations exchanged (see figure 11). Similar to our previous discussion, in this case, we can estimate an engine efficiency of $\eta \sim 1 - \omega_m/|\Delta_f|$. An example of the performance of this engine is reported in figure 12. The results reported in figures 12(a) and (b) are

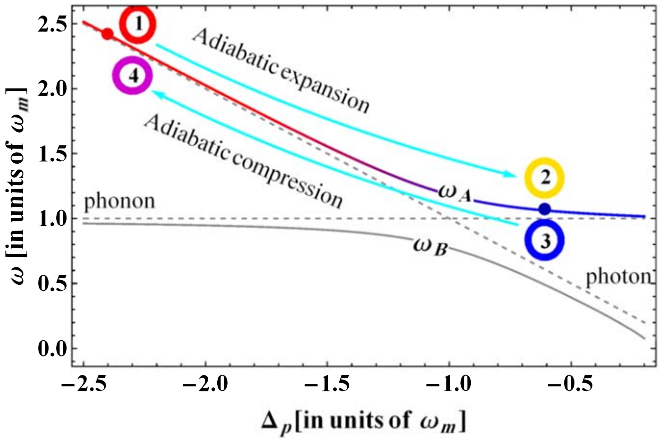

Figure 11. Scheme of the Otto cycle operated on the upper polariton (see figure 2 for the cycle operated on the lower polariton).

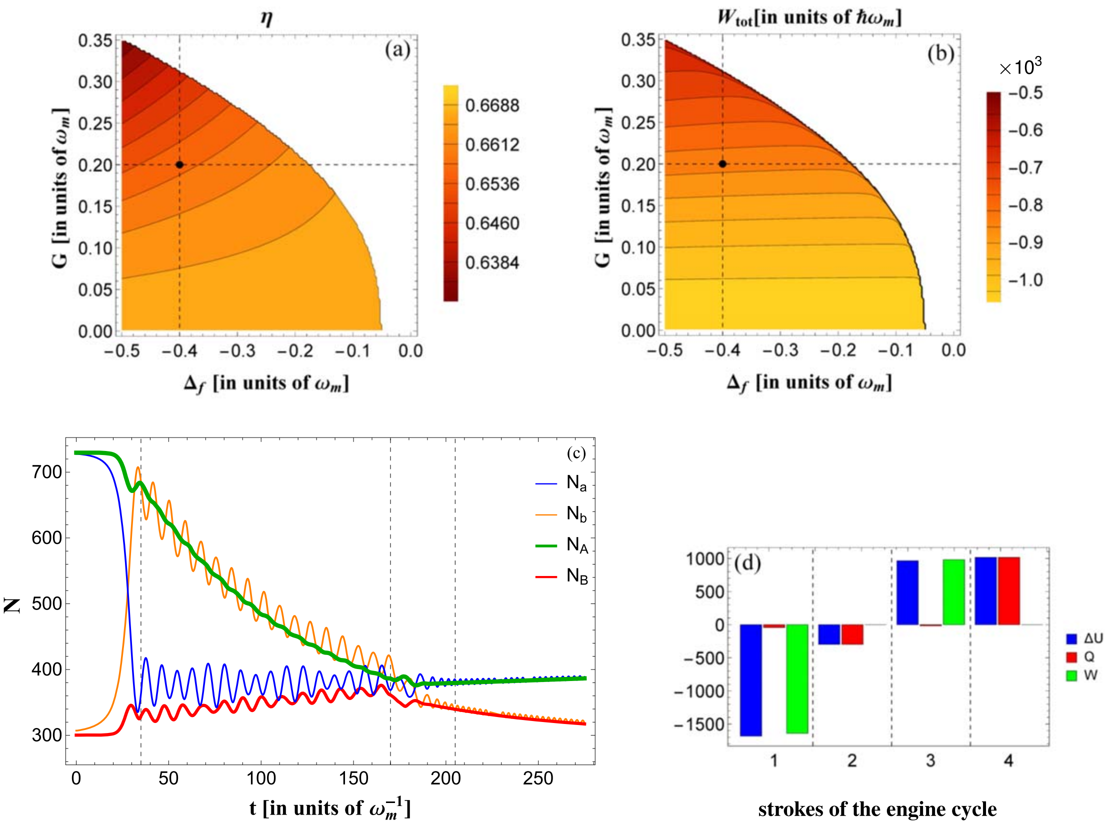

Figure 12. (a) Thermal efficiency η and (b) total work W_{tot} done by the engine (operated on the upper polariton) as a function of the Detuning Δ_f and the optomechanical coupling strength G, evaluated in terms of the steady-state quantities corresponding to the upper polariton at each node of the cycle, and assuming perfect adiabatic processes. The white ares indicate the parameters at which the system is unstable (see appendix C). The dots indicate the parameters used for the results in plots (c) and (d). (c) Shows the time evolution of the populations of the polariton and bare modes. (d) Shows the corresponding energy changes (blue), heat exchanged (red) and work performed (green) during each stroke of the cycle. The duration of each stroke is $\tau_1 = \tau_3 = 35\omega_m^{-1}$, $\tau_2 = 135\omega_m^{-1}$ and $\tau_4 = 20/\kappa_{\mathrm{fb}}$. The other parameters are $\Delta_i = -3\omega_m$, $2\kappa_c = 0.1\omega_m$, $2\gamma = 0.012\ \omega_m$, and $n_{th} = 300$. The feedback is set in order to achieve the effective cavity decay rate $2\kappa_{\mathrm{fb}} = 2 \times 10^{-4}\ \omega_m$ and the effective number of thermal photons $n_{\mathrm{opt,fb}} \approx 830$.

estimates evaluated in terms of the steady state energy of the upper polariton mode at each node of the stroke (assuming the population of the lower polariton mode constant). The efficiency in plot (a) is almost constant as a function of the final detuning Δ_f and this is due to the fact that the frequency of the upper polariton mode is almost constant for values of the detuning close to the cavity resonance (see figure 11). The plots in figures 12(c) and (d) are the time evolution of the modes populations and the heat and work corresponding to each stroke of the cycle for the parameters indicated by the dot in plots (a) and (b), and computed using the formulas presented in appendix C. They are qualitatively similar to the results of figures 5 (a) and (c) and demonstrate that for the chosen parameters the system is able to transform heat into work following an Otto cycle that involves only the upper polariton.

We finally remark that we have not found any significant qualitative and quantitative difference between the two schemes in the parameter regime that we have analysed (note that the higher efficiency in figure 12(d) as compared to figure 5(c) is due to the larger number of excitations used in the former). Furthermore we note that the scheme based on the upper polariton requires to run the feedback closer to the instability in order to achieve a sufficiently small $\kappa_{\rm fb}$ and a sufficiently large value of $n_{\rm opt,fb}$. This can make the experimental implementation of this engine significantly more problematic as compared to the engine based on the lower polariton.

6. Conclusion

Optomechanical devices come in very different sizes and configurations [5]. Their very high quality factor and the corresponding low natural mechanical decay rate, which is by far the lowest rate in the system dynamics, make them very versatile systems which are potential candidates for the experimental investigation of quantum thermodynamical effects. However, in spite of the many proposal of optomechanical based heat engine no experiment has demonstrated such devices so far. It is therefore important to suggest strategies for the realization of a working optomechanical quantum engine. Here we have shown that the experimental realization of the polariton-based quantum heat engine proposed in [7–9] can be significantly eased by means of a feedback system [16–19] which allows to control the decay rate of the optical cavity. This engine exploits the lower polariton mode as working fluid and works between the hot phononic thermal reservoir and the cold photonic reservoir with which the polariton comes into contact as the cavity pump detuning is varied around the red mechanical sideband frequency. A critical requirement in this device is the strong coupling regime, that corresponds to an optomechanical interaction strength larger then the cavity decay rate so that the polariton modes can be resolved. In general the coupling strength can be controlled by tuning the driving light power. While, in principle, this could allow to achieve the strong coupling regime, in practice it is often not possible to employ the needed power due to the onset of unwanted nonlinear effects. This is where the feedback realized in [16] can be helpful.

In this work, we have reported a detailed analysis of the performance of the engine when the feedback is employed to effectively reduce the cavity decay rates by driving the system close to the feedback instability threshold. We have demonstrated that the engine can work efficiently even if the system without feedback is not strongly coupled (such that in absence of feedback the polariton modes are not resolved). We have also shown that the feebdack noise, which can be seen as an effective non-zero temperature photonic bath, can be employed to define a similar engine working on the upper polariton mode where the role of the hot and cold baths are exchanged such that the feedback noise is absorbed as heat and transformed into usable work.

The feedback strategy that we have analysed seems easily applicable in any optomechanical system since it requires optical equipment already in use in most of optomechanical experiments. The results that we have presented correspond to systems in the resolved sideband regime and in cryogenic environments (considering a 1 MHz resonator the results in figures 3, 5, 6 and 12 would correspond to an external temperature of 100 mK, the results of figures 7–10, instead, would correspond to 1.7 K). Many experimental setups, both in the optical or microwave regimes, can be employed for demonstrating our proposal as for example [22–27]. In order to test the efficiency of this device one should be able to measure the energy variations and to distinguish the contributions due to heat and work. This can be done by measuring the correlation matrix of the system by following for example the approach realized in [24].

To conclude, we highlight that although we have not discussed specific quantum effects, the system that we have studied can be used to study such phenomena. An important example is the investigation of the effects of correlations in the reservoirs which have been predicted to enhance the efficiency of a quantum heat engine beyond the Carnot limit [28]. This could be in principle analysed with our optomechanical system by using, for example, a squeezed field to drive the cavity [26, 29]. Even more interestingly, in our case the bath correlations could be provided by the feedback loop itself [19]. Another related and important question is whether, correlations in the working fluid as well could be employed to enhance the efficiency of the engine as discussed in [30]. In our system, in fact, the feedback induced parametric term, which is negligible in the parameter regime that we have considered, could produce additional quantum coherence in the polariton state which may play a relevant role in certain situations. Finally, it is also interesting to ponder if, in some parameter regime, the behaviour of our engine could be interpreted as an instance of a Maxwell's demon [31] which, in fact, can be seen as a feedback system.

Acknowledgments

We acknowledge the support of the European Union Horizon 2020 Programme for Research and Innovation through the Project No. 732894 (FET Proactive HOT) and the Project QuaSeRT funded by the QuantERA ERA-NET Cofund in Quantum Technologies.

Appendix A. The model in matrix form and the correlation matrix

The quantum Langevin equations (2) and (9) can be rewritten in matrix form, in terms of the vector of operators $\underline{\hat{a}}^T = (\hat{a}, \hat{b}, \hat{a}^\dagger, \hat{b}^\dagger)$, as

$$\dot{\underline{\hat{a}}} = \mathcal{M}\underline{\hat{a}} + Q\,\underline{\hat{a}}_{\rm in}, \tag{A.1}$$

where the drift matrix is

$$\mathcal{M} = -\begin{pmatrix} \kappa_{\rm fb} - {\rm i}\Delta_p & {\rm i}G & \kappa_c - \kappa_{\rm fb} & {\rm i}G \\ {\rm i}G & \gamma + {\rm i}\omega_m & {\rm i}G & 0 \\ \kappa_c - \kappa_{\rm fb} & -{\rm i}G & \kappa_{\rm fb} + {\rm i}\Delta_p & -{\rm i}G \\ -{\rm i}G & 0 & -{\rm i}G & \gamma - {\rm i}\omega_m \end{pmatrix}, \tag{A.2}$$

the matrix Q is given by

$$Q = \begin{pmatrix} \sqrt{2\kappa_{\rm fb}} & 0 & 0 & 0 \\ 0 & \sqrt{2\gamma} & 0 & 0 \\ 0 & 0 & \sqrt{2\kappa_{\rm fb}} & 0 \\ 0 & 0 & 0 & \sqrt{2\gamma} \end{pmatrix}, \tag{A.3}$$

and $\underline{\hat{a}}_{\rm in}$ is the vector of noise operator $\underline{\hat{a}}_{\rm in}^{\rm T} = (\hat{a}_{\rm in}, \hat{b}_{\rm in}, \hat{a}_{\rm in}^\dagger, \hat{b}_{\rm in}^\dagger)$. From equation (A.1) one finds that the evolution of the correlation matrix

$$\mathcal{C} = \langle \underline{\hat{a}}\ \underline{\hat{a}}^T \rangle = \begin{pmatrix} \langle \hat{a}\hat{a} \rangle & \langle \hat{a}\hat{b} \rangle & \langle \hat{a}\hat{a}^\dagger \rangle & \langle \hat{a}\hat{b}^\dagger \rangle \\ \langle \hat{b}\hat{a} \rangle & \langle \hat{b}\hat{b} \rangle & \langle \hat{b}\hat{a}^\dagger \rangle & \langle \hat{b}\hat{b}^\dagger \rangle \\ \langle \hat{a}^\dagger\hat{a} \rangle & \langle \hat{a}^\dagger\hat{b} \rangle & \langle \hat{a}^\dagger\hat{a}^\dagger \rangle & \langle \hat{a}^\dagger\hat{b}^\dagger \rangle \\ \langle \hat{b}^\dagger\hat{a} \rangle & \langle \hat{b}^\dagger\hat{b} \rangle & \langle \hat{b}^\dagger\hat{a}^\dagger \rangle & \langle \hat{b}^\dagger\hat{b}^\dagger \rangle \end{pmatrix}, \tag{A.4}$$

is given by

$$\dot{\mathcal{C}} = \mathcal{M}\mathcal{C} + \mathcal{C}\mathcal{M}^T + Q\mathcal{C}_{\rm in}Q, \tag{A.5}$$

where $\mathcal{C}_{in}$ is the correlation matrix of the noise operators

$$\mathcal{C}_{\rm in} = \langle\, \underline{\hat{a}}_{\rm in}\ \underline{\hat{a}}_{\rm in}{}^T \rangle = \begin{pmatrix} 0 & 0 & n_{\rm opt,fb} + 1 & 0 \\ 0 & 0 & 0 & n_{\rm th} + 1 \\ n_{\rm opt,fb} & 0 & 0 & 0 \\ 0 & n_{\rm th} & 0 & 0 \end{pmatrix} \tag{A.6}$$

(note that in the absence of the feedback we have $\kappa_{\rm fb} = \kappa_c$ and $n_{\rm opt,fb} = 0$).

By defining $\mathcal{N} = Q\mathcal{C}_{\rm in}Q$ and introducing the linear super operator $\hat{\mathcal{L}}$ so that $\hat{\mathcal{L}}C = \mathcal{M}C + C\mathcal{M}^T$ we can find the stationary correlation matrix

$$\mathcal{C}_{ss} = -\hat{\mathcal{L}}^{-1}\mathcal{N}. \tag{A.7}$$

Appendix B. Polariton description of the system

The Hamiltonian corresponding to the quantum Langevin equations (2) and (9) is

$$\hat{H}_{\rm fb} = -\hbar\Delta_p\, \hat{a}^\dagger\hat{a} + \hbar\omega_m\hat{b}^\dagger\hat{b} + \hbar G(\hat{b} + \hat{b}^\dagger)(\hat{a} + \hat{a}^\dagger) - {\rm i}\,\hbar\,\frac{\kappa_c - \kappa_{\rm fb}}{2}(\hat{a}^2 - \hat{a}^{\dagger\,2}). \tag{B.1}$$

The uncoupled normal modes of $\hat{H}_{\rm fb}$, i.e. the polariton modes, can be expressed in terms of the bare operators $\hat{a}$ ($\hat{a}^\dagger$) and $\hat{b}$ ($\hat{b}^\dagger$) through a transformation matrix $\mathcal{T}$ as

$$\underline{\hat{A}} = \mathcal{T}^{-1}\underline{\hat{a}}, \tag{B.2}$$

where $\underline{\hat{A}} = (\hat{A}, \hat{B}, \hat{A}^\dagger, \hat{B}^\dagger)^T$ is the vector of the polariton operators and $\mathcal{T}$ is a symplectic transformation that satisfies the relations $\mathcal{T}\mathcal{I}\mathcal{T}^T = \mathcal{I}$ and $\mathcal{G}\mathcal{T}\mathcal{G} = \mathcal{T}^*$ where $\mathcal{T}^*$ is the matrix with the complex conjugate elements of $\mathcal{T}$, $\mathcal{G} = \begin{pmatrix} 0 & 1 \\ 1 & 0 \end{pmatrix}$, and $\mathcal{I}$ is the symplectic form $\mathcal{I} = \begin{pmatrix} 0 & 1 \\ -1 & 0 \end{pmatrix}$, with 1 the identity matrix. In terms of the polariton operators, the Hamiltonian (B.1) reads

$$\hat{H}_{\text{fb}} = \hbar\omega_A \hat{A}^\dagger \hat{A} + \hbar\omega_A \hat{B}^\dagger \hat{B} + \text{const}, \tag{B.3}$$

and the transformation matrix $\mathcal{T}$ can be obtained by solving the eigenvalue problem

$$\mathcal{M}_0\, \mathcal{T} = \mathcal{T}\mathcal{D}, \tag{B.4}$$

where, $\mathcal{M}_0 = \mathcal{I}\mathcal{H}$ with $\mathcal{H}$ the matrix representation of equation (B.1), i.e. $\hat{H}_{\text{fb}} = \underline{\hat{a}}^T \mathcal{H} \underline{\hat{a}}$, given by

$$\mathcal{H} = \frac{\hbar}{2}\begin{pmatrix} -\mathrm{i}(\kappa_c - \kappa_{\text{fb}}) & G & -\Delta_p & G \\ G & 0 & G & \omega_m \\ -\Delta_p & G & \mathrm{i}(\kappa_c - \kappa_{\text{fb}}) & G \\ G & \omega_m & G & 0 \end{pmatrix}, \tag{B.5}$$

and $\mathcal{D}$ the diagonal matrix of symplectic eigenvalues, defined as $\mathcal{D} = \frac{1}{2}\,\text{diag}\{\omega_A, \omega_B, -\omega_A, -\omega_B\}$ where

$$\omega_A = \frac{1}{\sqrt{2}}\sqrt{\Delta_p^2 - (\kappa_c - \kappa_{\text{fb}})^2 + \omega_m^2 + \sqrt{[\Delta_p^2 - (\kappa_c - \kappa_{\text{fb}})^2 - \omega_m^2]^2 - 16G^2\Delta_p\omega_m}}\,, \tag{B.6}$$

$$\omega_B = \frac{1}{\sqrt{2}}\sqrt{\Delta_p^2 - (\kappa_c - \kappa_{\text{fb}})^2 + \omega_m^2 - \sqrt{[\Delta_p^2 - (\kappa_c - \kappa_{\text{fb}})^2 - \omega_m^2]^2 - 16G^2\Delta_p\omega_m}}\,. \tag{B.7}$$

In figure 2, we have depicted these eigenfrequencies in the red detuning regime ($\Delta_p < 0$) where the beam-splitter interaction term of the Hamiltonian of equation (B.1) plays the dominant role [7]. The Hamiltonian (B.1) is stable, and the polariton modes can be defined, whenever the lowest eigenfrequency ω_B is real positive, i.e. when $\Delta_p < -2G^2/\omega_m - \sqrt{4G^4/\omega_m^2 + (\kappa_c - \kappa_{fb})^2}$.

The correlation matrix $\mathcal{C}_p$ for the polariton modes

$$\mathcal{C}_p = \langle \underline{\hat{A}}\, \underline{\hat{A}}^T \rangle = \begin{pmatrix} \langle \hat{A}\hat{A} \rangle & \langle \hat{A}\hat{B} \rangle & \langle \hat{A}\hat{A}^\dagger \rangle & \langle \hat{A}\hat{B}^\dagger \rangle \\ \langle \hat{B}\hat{A} \rangle & \langle \hat{B}\hat{B} \rangle & \langle \hat{B}\hat{A}^\dagger \rangle & \langle \hat{B}\hat{B}^\dagger \rangle \\ \langle \hat{A}^\dagger\hat{A} \rangle & \langle \hat{A}^\dagger\hat{B} \rangle & \langle \hat{A}^\dagger\hat{A}^\dagger \rangle & \langle \hat{A}^\dagger\hat{B}^\dagger \rangle \\ \langle \hat{B}^\dagger\hat{A} \rangle & \langle \hat{B}^\dagger\hat{B} \rangle & \langle \hat{B}^\dagger\hat{A}^\dagger \rangle & \langle \hat{B}^\dagger\hat{B}^\dagger \rangle \end{pmatrix}, \tag{B.8}$$

is related to the bare modes correlation matrix by the relation

$$\mathcal{C}_p = \mathcal{T}^{-1}\mathcal{C}(\mathcal{T}^{-1})^T. \tag{B.9}$$

In particular the steady state in the polariton base is obtained by computing equation (B.9) on the steady state correlation matrix (A.7). The steady state population of the polariton B is then given by the element (4, 2) of the resulting matrix (see (B.8)), i.e. $N_B = \{\mathcal{C}_p\}_{4,2}$, and similarly $N_A = \{\mathcal{C}_p\}_{3,1}$.

Appendix C. Heat and work

The internal energy U of the system can be expressed in terms of the average of the system Hamiltonian [1]

$$U(t) = \langle \hat{H}_{\text{fb}}(t) \rangle = \text{Tr}[\hat{\rho}(t)\hat{H}_{\text{fb}}(t)] \tag{C.1}$$

where $\rho(t)$ is the density matrix which describes the state of the system at time t, and $H_{\text{fb}}(t)$ is the system Hamiltonian (B.1), with time dependent detuning $\Delta_p(t)$. The energy change is given by the temporal derivative of the internal energy

$$\dot{U}(t) = \text{Tr}[\hat{\rho}(t)\dot{\hat{H}}(t)] + \text{Tr}[\dot{\hat{\rho}}(t)\hat{H}(t)], \tag{C.2}$$

which is the sum of two contributions. The first, associated with the variation of the system Hamiltonian, contributes to the work, while the second one is due to irreversible dissipative processes and contributes to the heat [32]. Specifically, in a process that takes place from the initial time t_i to the final time t_f, the heat Q and the work W are defined by the time integrals

$$Q = \int_{t_i}^{t_f} \mathrm{d}t\ \text{Tr}[\dot{\hat{\rho}}(t)\hat{H}_{\text{fb}}(t)], \tag{C.3}$$

$$W = \int_{t_i}^{t_f} \mathrm{d}t\ \mathrm{Tr}[\hat{\rho}(t)\dot{\hat{H}}_{\mathrm{fb}}(t)], \tag{C.4}$$

such that

$$Q + W = \Delta U \tag{C.5}$$

which represent the first law of thermodynamics. The difference in internal energy ΔU can be computed in terms of the average values of the system Hamiltonian (B.1), as $\Delta U = \langle H_{\mathrm{fb}}(t_f)\rangle - \langle H_{\mathrm{fb}}(t_i)\rangle$. In particular, the average value $\langle H_{\mathrm{fb}}(t)\rangle$ can be expressed in terms of the second order correlation functions (which in turn are derived using the solution of the equation for the correlation matrix (A.5) evaluated using the time dependent detuning (19)) as

$$\begin{aligned}\langle \hat{H}_{\mathrm{fb}}(t)\rangle = &-\hbar\Delta_p(t)\langle \hat{a}^\dagger(t)\ \hat{a}(t)\rangle + \hbar\omega_m\langle \hat{b}^\dagger(t)\ \hat{b}(t)\rangle\\ &+ \hbar G[\langle \hat{b}(t)\ \hat{a}(t)\rangle + \langle \hat{b}(t)\ \hat{a}^\dagger(t)\rangle + \langle \hat{b}^\dagger(t)\ \hat{a}(t)\rangle + \langle \hat{b}^\dagger(t)\ \hat{a}^\dagger(t)\rangle]\\ &- \mathrm{i}\,\hbar\,\frac{\kappa_c - \kappa_{\mathrm{fb}}}{2}[\langle \hat{a}(t)^2\rangle - \langle \hat{a}^\dagger(t)^2\rangle].\end{aligned} \tag{C.6}$$

The heat, instead, can be computed by substituting the system Hamiltonian (B.1) and the system master equations

$$\begin{aligned}\dot{\hat{\rho}} = &-\frac{\mathrm{i}}{\hbar}[\hat{H}_{\mathrm{fb}}(t), \hat{\rho}] + \kappa_c(n_{\mathrm{opt,fb}} + 1)(2\hat{a}\hat{\rho}\hat{a}^\dagger - \hat{a}^\dagger\hat{a}\hat{\rho} - \hat{\rho}\hat{a}^\dagger\hat{a}) + \kappa_c\ n_{\mathrm{opt,fb}}(2\hat{a}^\dagger\hat{\rho}\hat{a} - \hat{a}\hat{a}^\dagger\hat{\rho} - \hat{\rho}\hat{a}\hat{a}^\dagger)\\ &+ \gamma(n_{\mathrm{th}} + 1)(2\hat{b}\hat{\rho}\hat{b}^\dagger - \hat{b}^\dagger\hat{b}\hat{\rho} - \hat{\rho}\hat{b}^\dagger\hat{b}) + \gamma n_{\mathrm{th}}(2\hat{b}^\dagger\hat{\rho}\hat{b} - \hat{b}\hat{b}^\dagger\hat{\rho} - \hat{\rho}\hat{b}\hat{b}^\dagger)\end{aligned} \tag{C.7}$$

(which provides a description of the system dynamics equivalent to the quantum Langevin equations (2) and (9)), into equation (C.3). Thereby, exploiting the cyclic property of the trace, one finds that the heat exchanged with the environment in a process from time t_i to t_f is given by

$$\begin{aligned}Q = &\int_{t_i}^{t_f} \mathrm{d}t\ \mathrm{Tr}[\dot{\hat{\rho}}(t)\hat{H}_{\mathrm{fb}}(t)] = \int_{t_i}^{t_f} \mathrm{d}t\ \{2\hbar\omega_m\gamma n_{\mathrm{th}} - 2\hbar\Delta_p(t)\kappa_c n_{\mathrm{opt}} + 2\hbar\Delta_p(t)\kappa_c\langle \hat{a}^\dagger(t)\ \hat{a}(t)\rangle\\ &- 2\hbar\omega_m\gamma\kappa_c\langle \hat{b}^\dagger(t)\ \hat{b}(t)\rangle\\ &- \hbar G(\kappa_c + \gamma)[\langle \hat{b}(t)\ \hat{a}(t)\rangle + \langle \hat{b}(t)\ \hat{a}^\dagger(t)\rangle + \langle \hat{b}^\dagger(t)\ \hat{a}(t)\rangle + \langle \hat{b}^\dagger(t)\ \hat{a}^\dagger(t)\rangle]\\ &+ \mathrm{i}\hbar\ \kappa_c\ (\kappa_c - \kappa_{\mathrm{fb}})[\langle \hat{a}(t)^2\rangle - \langle \hat{a}^\dagger(t)^2\rangle]\}.\end{aligned} \tag{C.8}$$

The correlation functions in this expression can be computed by solving the equation for the correlation matrix (A.5) (with the time dependent detuning). Finally, the work is determined, in terms of these results for ΔU and Q, using the first law of thermodynamics (C.5).

We notice that this approach allows to extend the numerical analysis introduced in [7–9] (which, being based on the numerical integration of the master equation, is constrained to a low number of system excitations) to an arbitrary number of excitations.

References

[1] Vinjanampathy S and Anders J 2016 Quantum thermodynamics *Contemp. Phys.* **57** 545–79
[2] Alicki R and Kosloff R 2018 Introduction to quantum thermodynamics: history and prospects arXiv:1801.08314 [quant-ph]
[3] Bowen W P and Milburn G J 2015 *Quantum Optomechanics* (London: Taylor and Francis)
[4] Li B-B, Bílek J, Hoff U B, Madsen L S, Forstner S, Prakash V, Schäfermeier C, Gehring T, Bowen W P and Andersen U L 2018 Quantum enhanced optomechanical magnetometry *Optica* **5** 850
[5] Aspelmeyer M, Kippenberg T J and Marquardt F 2014 Cavity optomechanics *Rev. Mod. Phys.* **86** 1391–452
[6] Bawaj M *et al* 2015 Probing deformed commutators with macroscopic harmonic oscillators *Nat. Commun.* **6** 7503
[7] Zhang K, Bariani F and Meystre P 2014 Quantum optomechanical heat engine *Phys. Rev. Lett.* **112** 150602
[8] Zhang K, Bariani F and Meystre P 2014 Theory of an optomechanical quantum heat engine *Phys. Rev.* A **90** 023819
[9] Dong Y, Zhang K, Bariani F and Meystre P 2015 Work measurement in an optomechanical quantum heat engine *Phys. Rev.* A **92** 033854
[10] Dong Y, Bariani F and Meystre P 2015 Phonon cooling by an optomechanical heat pump *Phys. Rev. Lett.* **115** 223602
[11] Dechant A, Kiesel N and Lutz E 2015 All-optical nanomechanical heat engine *Phys. Rev. Lett.* **114** 183602
[12] Mari A, Farace A and Giovannetti V 2015 Quantum optomechanical piston engines powered by heat *J. Phys. B: At. Mol. Opt. Phys.* **48** 175501
[13] Gelbwaser-Klimovsky D and Kurizki G 2015 Work extraction from heat-powered quantized optomechanical setups *Sci. Rep.* **5** 07809
[14] Bathaee M and Bahrampour A R 2016 Optimal control of the power adiabatic stroke of an optomechanical heat engine *Phys. Rev.* E **94** 022141
[15] Zhang K and Zhang W 2017 Quantum optomechanical straight-twin engine *Phys. Rev.* A **95** 053870
[16] Rossi M, Kralj N, Zippilli S, Natali R, Borrielli A, Pandraud G, Serra E, Di Giuseppe G and Vitali D 2018 Normal-mode splitting in a weakly coupled optomechanical system *Phys. Rev. Lett.* **120** 073601
[17] Rossi M, Kralj N, Zippilli S, Natali R, Borrielli A, Pandraud G, Serra E, Di Giuseppe G and Vitali D 2017 Enhancing sideband cooling by feedback-controlled light *Phys. Rev. Lett.* **119** 123603

[18] Kralj N, Rossi M, Zippilli S, Natali R, Borrielli A, Pandraud G, Serra E, Di Giuseppe G and Vitali D 2017 Enhancement of three-mode optomechanical interaction by feedback-controlled light *Quantum Sci. Technol.* **2** 034014

[19] Zippilli S, Kralj N, Rossi M, Di Giuseppe G and Vitali D 2018 Cavity optomechanics with feedback-controlled in-loop light *Phys. Rev.* A **98** 023828

[20] De Angelis G V 2018 Optomechanical heat engine with feedback-controlled light *Master Thesis* Università degli studi di Camerino, Camerino

[21] Gardiner C and Zoller P 2004 *Quantum Noise: A Handbook of Markovian and Non-Markovian Quantum Stochastic Methods with Applications to Quantum Optics, Springer Series in Synergetics* 3rd edn (Berlin: Springer)

[22] Gröblacher S, Hertzberg J B, Vanner M R, Cole G D, Gigan S, Schwab K C and Aspelmeyer M 2009 Demonstration of an ultracold micro-optomechanical oscillator in a cryogenic cavity *Nat. Phys.* **5** 485–8

[23] Teufel J D, Li D, Allman M S, Cicak K, Sirois A J, Whittaker J D and Simmonds R W 2011 Circuit cavity electromechanics in the strong-coupling regime *Nature* **471** 204–8

[24] Palomaki T A, Teufel J D, Simmonds R W and Lehnert K W 2013 Entangling mechanical motion with microwave fields *Science* **342** 710–3

[25] Peterson R W, Purdy T P, Kampel N S, Andrews R W, Yu P-L, Lehnert K W and Regal C A 2016 Laser cooling of a micromechanical membrane to the quantum backaction limit *Phys. Rev. Lett.* **116** 063601

[26] Clark J B, Lecocq F, Simmonds R W, Aumentado J and Teufel J D 2017 Sideband cooling beyond the quantum backaction limit with squeezed light *Nature* **541** 191–5

[27] Shomroni I, Qiu L, Malz D, Nunnenkamp A and Kippenberg T J 2019 Optical backaction-evading measurement of a mechanical oscillator *Nat. Commun.* **10** 2086

[28] Niedenzu W, Mukherjee V, Ghosh A, Kofman A G and Kurizki G 2018 Quantum engine efficiency bound beyond the second law of thermodynamics *Nat. Commun.* **9** 165

[29] Asjad M, Zippilli S and Vitali D 2016 Suppression of Stokes scattering and improved optomechanical cooling with squeezed light *Phys. Rev.* A **94** 051801

[30] Klatzow J, Becker J N, Ledingham P M, Weinzetl C, Kaczmarek K T, Saunders D J, Nunn J, Walmsley I A, Uzdin R and Poem E 2019 Experimental demonstration of quantum effects in the operation of microscopic heat engines *Phys. Rev. Lett.* **122** 110601

[31] Lloyd S 1997 Quantum-mechanical Maxwell's demon *Phys. Rev.* A **56** 3374–82

[32] Alicki R 1979 The quantum open system as a model of the heat engine *J. Phys. A: Math. Gen.* **12** L103–7